Title

Recombination activity of threading dislocations in GaInP influenced by growth temperature

Journal

Journal of Applied Physics, 123(16)

ISSN

0021-8979

Authors

Mukherjee, K
Reilly, CH
Callahan, PG
et al.

Publication Date

2018-04-28

DOI

10.1063/1.5018849

Peer reviewed

Recombination activity of threading dislocations in GaInP influenced by growth temperature

K. Mukherjee[1], C. H. Reilly[1], P. G. Callahan[1], G. G. E. Seward[2]

[1]Materials Department, University of California, Santa Barbara, CA 93106, U.S.A

[2]Department of Earth Science, University of California, Santa Barbara, CA 93106, U.S.A

Abstract

Room-temperature non-radiative recombination is studied at single dislocations in $Ga_{0.5}In_{0.5}P$ quantum wells grown on metamorphic templates using cathodoluminescence and electron channeling contrast imaging. An analysis of the light emission intensity profiles around single dislocations reveals that the average recombination strength of a dislocation decreases by a factor of four and seven as a result of decreasing the growth temperature of the GaInP quantum well from 725 to 675 and 625 °C respectively. This reduction occurs despite little change in the diffusion length, precluding the prospect of inducing carrier localization by ordering and phase separation in GaInP at lower growth temperatures. These observations are rationalized by the premise that point defects or impurities are largely responsible for the recombination activity of dislocations, and the extent of decoration of the dislocation core decreases with temperature. Preliminary evidence for the impact of the Burgers vector is also presented. The lowest growth temperature, however, negatively impacts light emission away from dislocations. Carrier recombination in the bulk and at dislocations need to be considered together for metamorphic devices, and this work can lead to new techniques to limit non-radiative recombination.

I. INTRODUCTION

The generation of dislocations to accommodate lattice constant-mismatch or thermal expansion coefficient-mismatch to a substrate is common in many epitaxial films. Among semiconducting materials, mismatched epitaxial films have immense technological importance. Examples include SiGe and InGaAs on Si for logic[1,2], InGaAs and GaInP on GaAs for optoelectronics and photovoltaics,[3] and InGaN on sapphire for solid-state lighting.[4] However, dislocations are known to degrade both the performance and lifetime of such devices. The most common and successful technique to improve the performance of mismatched devices has been to reduce the number of dislocations in the active region. An alternative approach, and the one followed in this paper, is to reduce non-radiative carrier recombination on an individual dislocation basis, which is then characterized. There are two reasons why this approach is not common—(1) factors controlling non-radiative recombination at dislocations are neither well understood nor easy to control and (2) modifications made to the material to reduce non-radiative recombination could deleteriously impact radiative recombination even away from dislocations. This paper represents a step towards understanding these factors with the help of systematically introduced growth modifications and a novel combination of scanning electron beam characterization techniques.

Certain types of materials exhibit carrier localization, which manifests as a lower carrier diffusivity or mobility. This phenomenon has been very successful in providing a degree of isolation from dislocations in the III-nitride blue and green LEDs and laser diodes.[5] Similarly, artificially-induced carrier localization offered by InAs quantum dots provides exceptional immunity from dislocations, leading to reliable infrared lasers on silicon.[6] In this study, we examine if the diffusion length can be lowered by the less drastic, tunable, microstructural inhomogeneities that have been previously reported to exist in III-phosphide semiconductors. This

would enable heterogeneous integration of red and amber LEDs and laser diodes on cost-effective substrates. $Ga_{0.5}In_{0.5}P$ has the potential for carrier localization at low growth temperatures due to the presence of phase separation and ordering, with reports of band edge fluctuations of ~50 meV.[7] However, the effect of this on dislocation recombination has not yet been studied. Here, the impact of individual dislocations on red light emission is measured as a function of the growth temperature of a GaInP quantum well. In summary, while we did observe a reduction in the impact of dislocations at lower growth temperatures, this occurred without a change in the carrier diffusion length—implying a change in the recombination activity at the dislocation core itself. We conclude that the recombination property of a dislocation is likely dictated by impurities. However, the extent to which impurities are able to decorate dislocations depends on the processing conditions and potentially also the Burgers vector. In other words, the recombination activity of a dislocation in GaInP, and likely other semiconductors, is not fixed. This opens up potential ways of engineering the properties of dislocations in semiconductors.

II. EXPERIMENT AND METHODS

A. Sample structure and growth parameters

Samples were synthesized in a Thomas Swan/AIXTRON low-pressure metal-organic chemical vapor deposition (LP-MOCVD) system with a close-coupled showerhead. The growth pressure was fixed at 100 Torr and purified N_2 was used as the carrier gas. Quantum wells with a nominal composition of $Ga_{0.5}In_{0.5}P$ (hereafter referred to as GaInP) with a thickness of 5 nm were synthesized with $Al_{0.5}In_{0.5}P$ and $(Al_{0.7}Ga_{0.3})_{0.5}In_{0.5}P$ barriers, lattice-matched to (001)-oriented GaAs substrates. The input V/III ratio of the III-phosphide layers was approximately 400. The quantum-wells and the barrier layers were not intentionally doped. Three different samples were grown at temperatures of 725, 675, and 625 °C respectively for the quantum well and 750 °C for

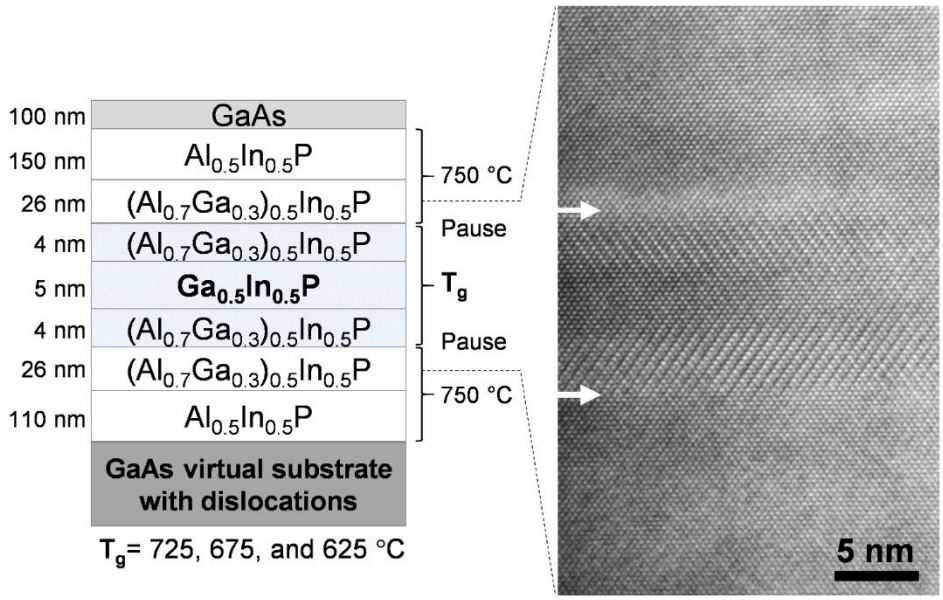

Fig. 1. Sample design and high resolution TEM of the quantum-well region showing double-variant CuPt type-B ordering in the AlGaInP barrier and GaInP well (shown for T_g=675 °C, [110] projection). The white arrows correspond to the growth pause locations. The process used to create the dislocations in the virtual substrate is described in the text.

all other phosphide layers. Fig. 1 shows a schematic and a 200 kV TEM image (JEOL JEM-2011) of the sample grown at 675 °C showing CuPt-B ordering in the quantum well. Lowering the temperature for the quantum well required a growth pause under PH_3 atmosphere for up to 200 seconds. To avoid the potential for impurities at the quantum-well/barrier interface, the growth pause was introduced 4 nm into the barriers.

This structure deposited directly on a GaAs substrate would have a very low threading dislocation density. Therefore, in this experiment we used compositionally graded buffers to create a virtual substrate with a high density of threading dislocations. An InGaAs compositionally graded buffer was used to compressively-grade (2.6% strain/μm) from the GaAs lattice constant to $In_{0.15}Ga_{0.85}As$, followed by a 200 nm constant composition layer of $In_{0.15}Ga_{0.85}As$, returning to the GaAs lattice constant with a tensile-graded (2.6% strain/μm) InGaAs buffer. This was followed by nearly 1 μm of lattice-matched arsenide growth, which included a GaAs/AlGaAs quantum well

for diagnostic purposes. Under conditions of ideal dislocation glide, the threading dislocation density is proportional to the grading rate and offers a pathway to controllably introduce dislocations in an otherwise well-characterized material system. This is important because accurate characterization of the dislocation recombination activity requires the use of semiconductor parameters such as the carrier lifetime and mobility from dislocation-free samples. The grading rate for the tensile graded buffer in this study was un-optimized and led to significant dislocation pile-ups and non-uniformity. Even in regions away from pile-ups, this led to different threading dislocation densities in the range of $(1-4)\times 10^{7}/cm^{2}$ in the three samples. Nevertheless, the samples lent themselves well to the study of dislocation recombination activity, which was the focus of this study. It is anticipated that the recombination properties of these 'clean' dislocations would be similar to that for growth on lattice-mismatched substrates such as Si or GaP.

B. Cathodoluminescence and electron channeling contrast imaging

Cathodoluminescence (CL) spectroscopy and electron channeling contrast imaging (ECCI) were performed using an FEI Quanta 400F at 30 kV. Electron channeling images were acquired not only to gain an insight into the correlation between defect-type and light emission, but also to ensure that the analysis was performed on isolated single dislocations and not a closely spaced group of dislocations. This is especially an issue for the III-arsenide and III-phosphide materials, with longer diffusion lengths than the III-nitrides. The probe current was set to 3–4 nA for both ECCI and panchromatic CL imaging. The cathodogenerated carrier concentration was estimated to be in the $10^{18}/\text{cm}^3$ range, comparable to high brightness LEDs and laser diodes. CL spectra were measured using a silicon CCD array at a higher probe current of 70 nA and the emission intensity was normalized to the underlying reference GaAs quantum well—which is nominally the same in all three samples. Panchromatic CL signal was collected using an elliptical mirror and detected

using a photomultiplier tube (PMT, ET Enterprises) that is insensitive to light beyond 700 nm, such as that from the GaAs layers. The CL signal from the photomultiplier was verified for linearity after removing DC offsets in the amplifier circuit, crucial for obtaining accurate contrast profiles. This was done by noting that the measured dislocation contrast was independent of the gain of the PMT. ECCI was performed in backscatter mode using a pole-piece mounted solid state detector at a working distance of 5–6 mm in both the three-beam ($g = 004, 02\bar{2}$) and a few different two-beam conditions. ECCI, like TEM, is a technique based on electron diffraction and can be used in a two-beam geometry where only one reciprocal lattice vector satisfies the Bragg condition.[8–11] Threading dislocations with different Burgers vectors exhibit different dark-light contrast based on the g-vector used. However, identification of the Burgers vectors of threading dislocations was not performed in this study as the invisibility criteria are often inapplicable due to surface relaxation and would have necessitated defect contrast simulation which is beyond the scope of this paper.[12]

C. Estimating diffusion lengths and the dislocation recombination activity

The CL contrast at a dislocation depends on transport and recombination parameters of defect-free versions of the semiconductor or equivalently that of regions away from dislocations. Additionally, it also depends on dislocation-specific properties and the SEM imaging conditions. In order to de-convolve these parameters, line plots of the CL intensity at individual dislocations were extracted from the CL images and compared to a phenomenological model of CL intensity at dislocations.[13] In this model, an analytical solution is obtained for CL intensity in thin films with a point source of carriers, a dislocation with arbitrary recombination strength, and front and back surfaces with arbitrary surface recombination velocities. We adapt this solution to our quantum wells with a few assumptions. The significantly lower interface recombination velocity at the quantum-well/barrier

interface[14] compared to a free surface was approximated by the condition of zero surface recombination at both the top and bottom interfaces (a reflection boundary condition for carriers). The normalized CL intensity as a function of radial position of the point source, r, from the dislocation is then given by:

$$I_{CL}(r) = 1 - \frac{K_0\left({}^{r}/_{L_d}\right)}{K_0\left({}^{R}/_{L_d}\right) + {}^{{L_d}^2}/_{RS\tau}} \qquad (1)$$

where K_0 is the first order modified Bessel function of the second kind, L_d is the carrier diffusion length, equal to $\sqrt{D\tau}$, where D is the diffusivity and τ is the carrier lifetime in the absence of dislocations. τ depends on the radiative (τ_R) and non-radiative recombination (τ_{NR}) lifetimes as $\tau = {}^{\tau_R\tau_{NR}}/_{(\tau_R + \tau_{NR})}$. R and S are two parameters pertaining to the dislocation—the radius of the cylinder of the dislocation core and the surface recombination velocity of that cylinder respectively. The entire expression reduces to a commonly used exponential decay away from the dislocation when $S \to \infty$.[15] While such an approximation is convenient to use, the exponential decay is often inaccurate near the dislocation core, can lead to inaccurate estimates of the diffusion length, and precludes further effort in understanding dislocations.[16] Even with the use of realistic values of recombination strengths in this study, it was not feasible to identify the values of R and S uniquely due to experimental uncertainties. Thus, the value of R was assumed to be constant and equal to 1 nm as has been done previously.[13]

Finally, the model setup to calculate CL intensity for a point source lends itself to convolution to account for a laterally diffuse source in the quantum well due to electron beam-sample interactions in CL. Ordinarily, the spread due to beam-sample interaction in bulk samples is lowest at low accelerating voltage. However, the proximity of the quantum well to the sample

surface and the presence of a back barrier allowed us to operate at 30 kV without sacrificing image resolution (indeed with better spatial resolution than lower voltages of 10–15 kV). A lateral source radius of 70 nm was obtained from Monte Carlo simulation of electron energy loss performed using Casino[17], which is small compared to typical diffusion lengths in GaInP. To arrive at this value, it was assumed that only energy loss in the AlInP barriers and GaInP quantum-well layers results in carriers in the quantum well. Lateral diffusion of carriers in the AlInP barrier was not factored into this calculation.

III. RESULTS

A. Luminescence away from dislocations

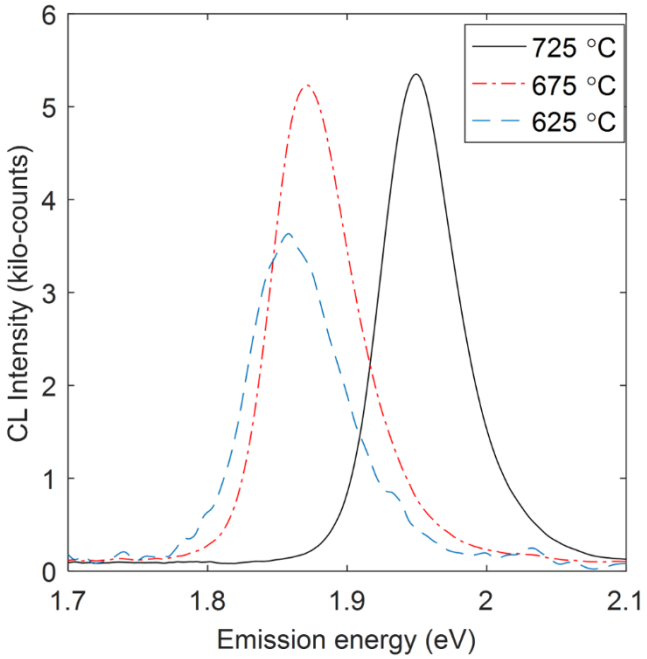

Fig. 2. Room temperature cathodoluminescence (CL) spectra collected from point-source excitation at a region away from dislocations. The emission energy is seen to decrease with a reduction in growth temperature due to the introduction of ordering and phase separation in GaInP. The emission intensity is also lower for the coldest sample.

If a reduction in the growth temperature reduces the emission intensity in dislocation-free samples, this would limit its use as a means to reduce the dislocation activity. To study this, room-

temperature CL spectra were collected from the samples using point-excitation at regions away from dislocations. The integrated CL intensity was also used to ascertain changes in the carrier lifetime, which is needed to quantify the dislocation recombination activity. Fig. 2 shows CL spectra from the three samples. A decrease in the peak emission energy of 80 and 90 meV is seen for the 675 °C and 625 °C growth temperatures respectively. This is comparable to other reports in the literature.[18] While we do not have an independent measurement of the relative contributions of ordering and phase separation to the decrease, ordering is expected to be largely responsible for the lowering in emission energy. The integrated CL intensities from the samples grown at 725 °C and 675 °C are very similar, in line with previous photoluminescence results with dislocation-free order/disorder quantum wells.[19] However, further reduction of the growth temperature of the quantum well to 625 °C results in a decline in CL intensity of 30%.

These trends in sample CL intensity away from dislocations can be explained by changes in τ_R as the growth temperature is decreased. This is based on conclusions derived from prior reports on lattice-matched GaInP samples, now applied to lattice-mismatched GaInP samples of the same composition. No direct lifetime measurements of the lattice-mismatched samples were conducted in this study. Unusually, ordered GaInP has been reported to have a longer τ compared to disordered GaInP.[20–23] This is contrary to expectations of shorter τ due to impurities when conventional semiconductors are grown colder. As an example, King et al. reported a near doubling in τ at room-temperature as GaInP was ordered.[24] Such ordered GaInP nevertheless resulted in external quantum efficiencies exceeding 90% in solar cells, suggesting that ordering is not inherently detrimental as long as τ_R continues to be significantly faster than τ_{NR}. The exact mechanism leading to a longer τ_R in ordered GaInP has not been established, but it is hypothesized to occur due to either a type-II band alignment[21,25,26] between ordered and disordered domains

within the material or a piezoelectric field in the ordered domains.[22,27] Recent time-resolved and continuous-wave photoluminescence measurements from similarly designed quantum-well samples grown in the same MOCVD chamber also showed a doubling in τ at room temperature with no reduction in emission intensity as the GaInP growth temperature was reduced from 750 °C (disordered) to 650 °C (ordered).[19] As there was no change in the CL intensity between 725 °C and 675 °C in this study, we interpreted this as a doubling of τ_R without much impact from a relatively longer τ_{NR}. This would lead to a doubling in $\tau \approx \tau_R$ but only a slight decrease in the quantum efficiency that is proportional to $\tau_{NR}/(\tau_{NR} + \tau_R)$ and is close to 0.9–1 for both growth temperatures. The growth temperature of 625 °C for the third sample is not particularly low and hence a lowering in the emission intensity due to a decrease in the non-radiative lifetime from impurities is not expected. Prior work on direct band gap AlInP in the same growth chamber showed no increase in oxygen incorporation as the growth temperature was lowered from 725 °C to 620 °C.[28] However, if τ_R continues to rise from a further increase in electron-hole separation due to the formation of larger ordered domains at 625 °C, it could become comparable to τ_{nr} and result in a lowering of the emission intensity. In previous work on ordered AlGaInP quantum wells, which are known to have a higher order parameter than GaInP, τ was seen to increase by nearly an order of magnitude at room temperature compared to the disordered case.[19]

Approximate values of $\tau = 1$, 2, and 5 ns were inferred for the samples grown at 725, 675, and 625 °C, respectively, based on the intensity results and lifetime results[19]. This is consistent with the CL intensity measurements assuming a constant $\tau_{NR} = 11$–13 ns across the samples. Note that we do not have a direct measurement of τ_{NR} and are unable to verify if τ_{NR} decreases slightly when the growth temperature is reduced. These values of τ were used in the determination of the

dislocation recombination activity using Eqn. 1. Further verification of increasing τ with decreasing growth temperature is shown in section III.B via the carrier diffusion lengths.

B. Recombination activity at individual dislocations

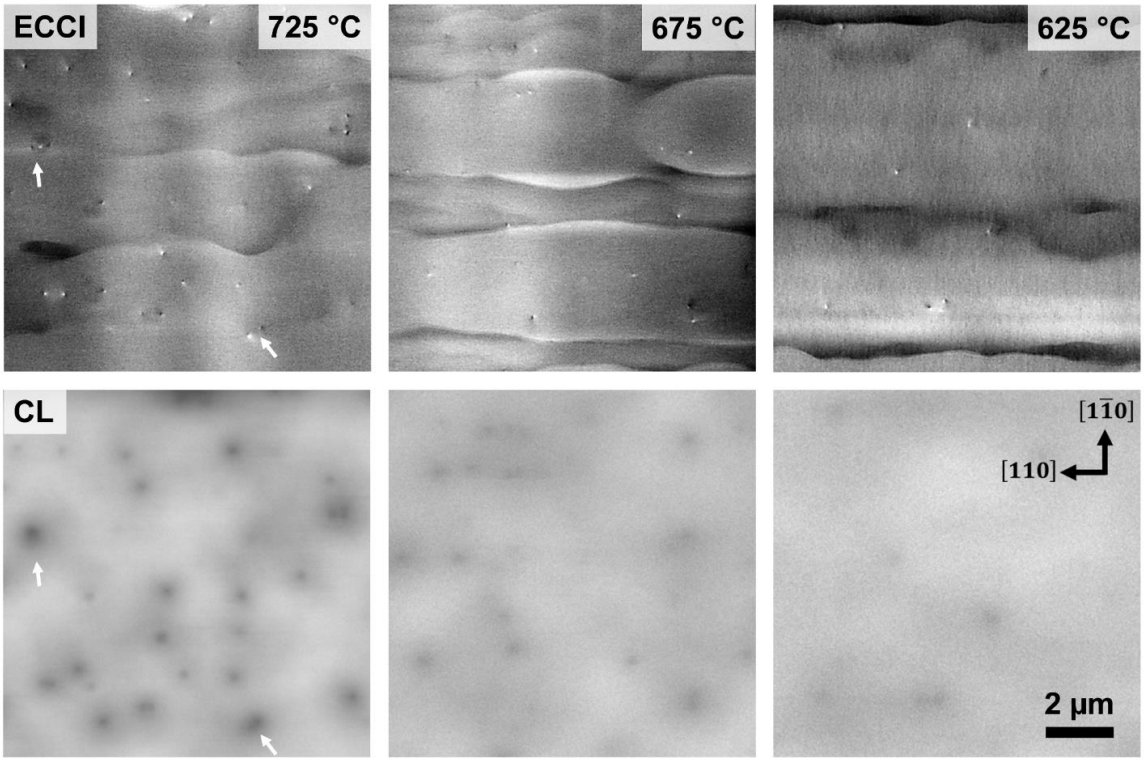

Fig. 3. Electron channeling contrast images (ECCI) in the three-beam ($g = 004, 02\bar{2}$) condition and corresponding panchromatic CL maps as a function of growth temperature. Threading dislocations in the ECCI images are visible as sharp dots with a light/dark contrast. A one-to-one link between threading dislocations and dark-spots in the CL image is established. White arrows point to two examples of closely spaced threading dislocations leading to overlapping CL dark-spots, such cases were excluded from the analysis. Overall, the CL contrast at dislocations appears to be reduced at lower growth temperatures.

A challenge with CL spectroscopy in non-nitride III-V semiconductors is the potential for overlap of the recombination regions of closely spaced dislocations, leading to misinterpretation of the recombination activity. To avoid this, we performed ECCI in addition to panchromatic CL imaging to characterize light emission from regions of isolated dislocations as a function of the growth

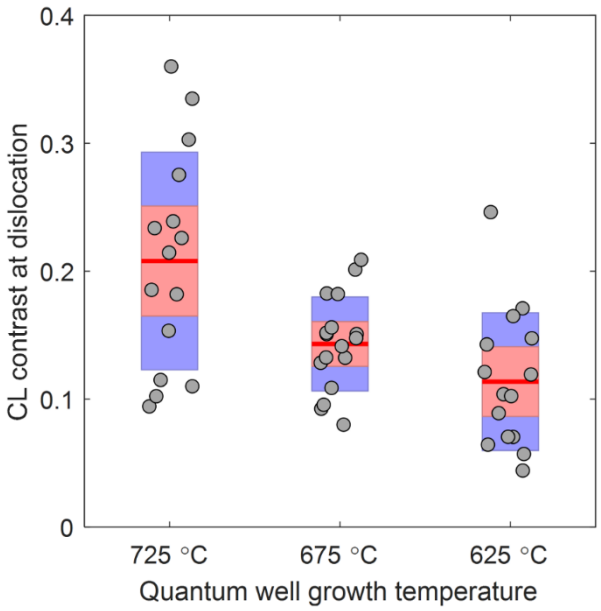

Fig. 4. CL contrast at dislocations for the three growth temperatures for ~15 isolated dislocations. The horizontal line represents the mean and the boxes represent one standard deviation and the 95% confidence interval.

temperature. Images from this process for the three samples are shown in Fig. 3, with white arrows pointing to typical closely spaced dislocations that were excluded from this study. Such coincident imaging using ECCI and CL was recently demonstrated in the nitride semiconductors.[29] The CL images have been normalized to unity at regions away from dislocations. Being almost equally bright, this scaling still allows for a direct comparison between the 725 °C and 675 °C samples, but not with the 625 °C sample which was less bright overall. Several threading dislocations are visible in all the samples on terraced surfaces, typical of lattice-mismatched GaInP. These dislocations are directly correlated to darker regions in the CL images, confirming that recombination at dislocations in GaInP is non-radiative in nature. Comparing the CL images across growth temperature, it is clear that lowering the growth temperature does in fact reduce CL contrast at dislocations. The CL dark spots at low growth temperatures are less well defined and not as easy to identify as they are in the 725 °C sample.

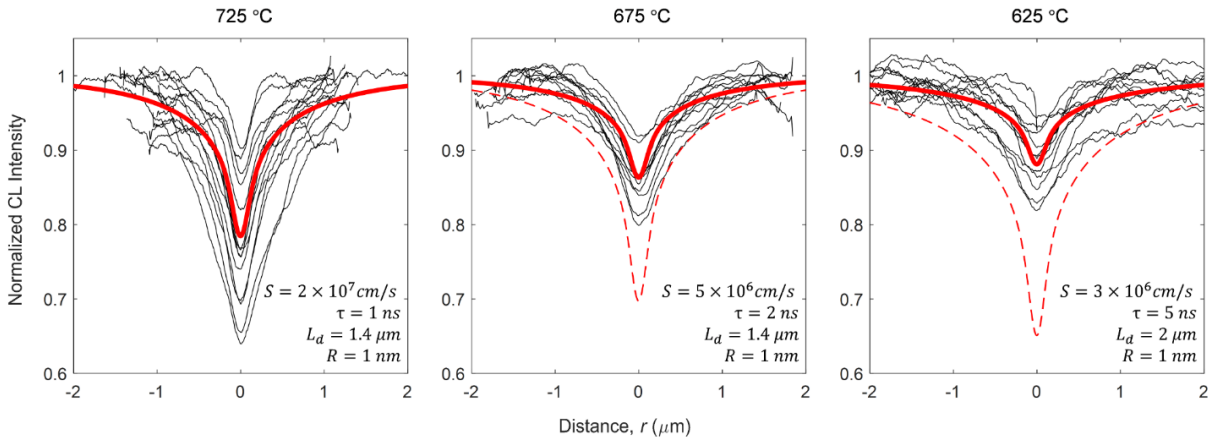

Fig. 5. Line profiles along $[1\bar{1}0]$ of CL intensity across ~15 dislocations as a function of sample growth temperature. The thick (red) line represents a fit using Eqn. 1 with the parameters listed. The dashed line represents the hypothetical CL output if the dislocation recombination velocity were to be unchanged from that at 725 °C.

To quantify this change in recombination activity, the CL contrast, defined as $(I - I_0)/I_0$, was extracted at ~15 isolated dislocations from each sample and is shown in Fig. 4. I_0 is the CL intensity away from dislocations. Overall, the sample grown at 675 °C has a lower mean value and a tighter distribution of CL contrast compared to that grown at 725 °C. The sample grown at 625 °C has an even lower mean contrast, with some dislocations difficult to detect in CL without use of ECCI. A significant spread in dislocation recombination activity is seen in all the samples, and is highest at 725 °C. This is found to be partially correlated to the dislocation structure, discussed further in III.C.

We now show that the reduced activity of dislocations in the 675 and 625 °C samples arises not from carrier localization away from dislocations but from a reduction in the recombination strength itself. To quantify the dislocation recombination activity in terms of a surface recombination velocity S of the dislocation cylinder, the model discussed in II.C was used, with the dislocation core radius arbitrarily set to $R = 1\,nm$ for all samples. τ and D for each growth temperature necessary for this analysis were estimated from measurements on dislocation-free

samples[19,30,31] and intensity measurements from regions away from dislocations as described in III.A. Measured CL intensity profiles along $[1\bar{1}0]$ from several individual dislocations are shown in Fig. 5 along with parameters used for the fit. Due to the significant spread in the dislocation recombination activity, the value of S was determined from a visual fit that represented the average behavior of the sample. The model output (Eqn. 1) is shown in red. The average recombination velocity S at the dislocation cylinder in the 725 °C sample is estimated to be $2 \times 10^7 cm/s$. The dislocation recombination strength, defined as $\gamma = 2\pi RS$,[32] is 13 cm^2/s. Remarkably, S is found to be lowered by a factor of 4 and 7 for the 675 °C and 625 °C samples respectively ($\gamma = 3.1$ and 1.8 cm^2/s respectively). To highlight the magnitude of this change, the dashed red lines show the calculated CL intensity profiles at 675 and 625 °C if S was unchanged from that in the 725 °C sample. It shows that if the dislocation activity were to be independent of growth temperature, they would actually be more deleterious at lower growth temperatures due to a longer τ leading to more carriers diffusing to the dislocation. Fig. 6 shows contour plots of CL intensity from representative single dislocations and provides further evidence that lowering the growth temperature modifies both transport and recombination. The elliptical nature of the contours characterizes an anisotropy in carrier diffusivity as high as 40% at 625 °C, with the direction of slow diffusivity corresponding to$[1\bar{1}0]$ —the direction along which Ga and In atoms are ordered. These results are equivalent to work by Haegel et al., in which anisotropy in carrier diffusion in ordered GaInP was imaged using a point source excitation.[30] In our work, the dislocations act as point sinks. Fitting to line-cuts along [110] did not significantly change the estimate for S in the anisotropic cases. To summarize, the diffusion lengths are either the same or increased at lower growth temperatures, indicative of no additional carrier localization. This is likely caused by the anomalous increase in τ as the order parameter is increased in GaInP. The longer τ completely counteracts a reduction in D. Thus, we

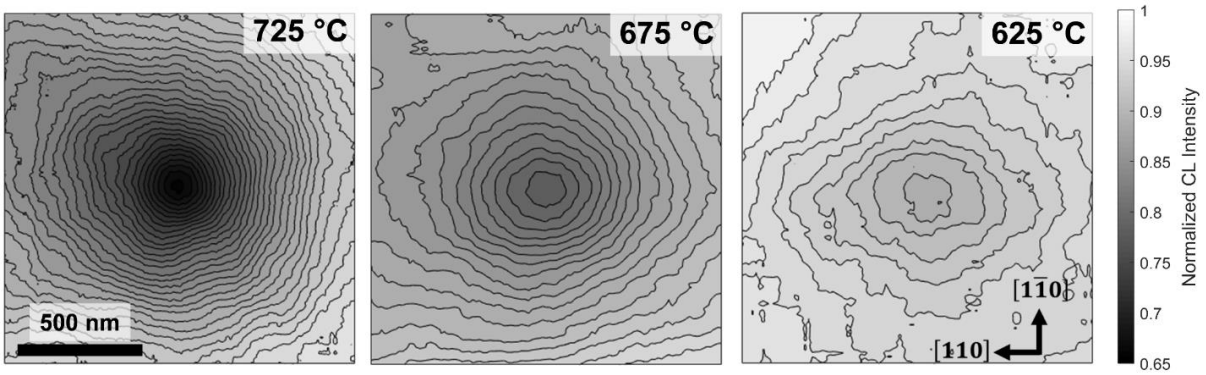

Fig. 6. Contour plots of normalized CL intensity around a single threading dislocation. The contour interval is 0.02. The anisotropy in diffusivity increases as the growth temperature is reduced. However, the diffusion length itself is not reduced due to an accompanying increase in carrier lifetime as the growth temperature is lowered.

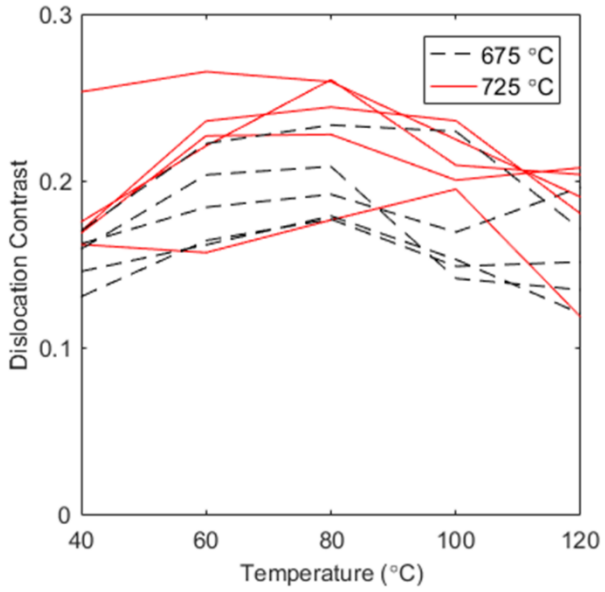

Fig. 7. Variation in the CL contrast from five isolated dislocations as a function of measurement temperature for samples grown at 725 °C (red, solid) and 675 °C (black, dashed).

conclude that it is the dislocation recombination activity itself that is reduced by lowering the growth temperature. Measurements on dislocation-free regions and samples make it possible to decouple the impact of growth temperature on the dislocation recombination strength and the bulk of the material. Thus, while the dislocation recombination activity is lowest at 625 °C, this is likely not ideal for device applications as the bulk away from dislocations also becomes inefficient. However, a case can be made for further exploring growths at intermediate temperatures, where

the dislocation activity is reduced without experiencing a noticeable change in the bulk efficiency at the studied injection level.

Finally, a comparison of the temperature dependence of the dislocation CL contrast between the samples grown at 725 °C and 675 °C is shown in Fig. 7. Five dislocations were selected at random from each sample and their contrast was tracked at sample stage temperatures of 40–120 °C. We conclude that there is no difference in the trend in contrast between the two samples, suggesting no difference in recombination mechanism.

C. Correlation of recombination activity with the dislocation structure

The significant variation in dislocation recombination activity even within a sample, seen in both Figs. 4 and 5, motivated a preliminary study of the underlying cause. Studies of dislocations in GaN highlighted the role of the Burgers vector in determining CL contrast.[33] On the other hand, an early CL study on GaP revealed all dark spot defects to be uniform—indicating no role of the Burgers vector.[34] To clarify this issue, we analyzed the dislocation CL contrast at ~170 individual dislocations from the sample grown at 725 °C (as it had the largest variation). A histogram of the contrast is presented in Fig. 8a. As histograms are sensitive to choice of bin-size and phase, we overlaid a probability density function using nonparametric kernel density estimation as implemented in MATLAB™. The histogram is scaled to the probability density function. This analysis shows a slight tendency towards bimodality in dislocation contrast, with approximately 10% of the dislocations behaving differently. The dashed lines in Fig. 8a show the two normal distributions that make up the bimodal distribution. Thus, it is seen that a majority of the dislocations follow a normal distribution with a very large spread in recombination activity.

The effect of the Burgers vector on the CL contrast was studied using ECCI. Fig. 8b shows a CL image and corresponding two-beam ECCI images from two pairs of dislocations, each close to the opposite end of the contrast distribution. The two dislocations exhibiting strong CL contrast are highlighted with white arrows in the CL image and marked by white boxes in the corresponding ECCI images. Similarly, the pair of dislocations with weak CL contrast are marked by black arrows and circles in the CL and ECCI images respectively. Fitting Eqn. 1 using the parameters in III.B,

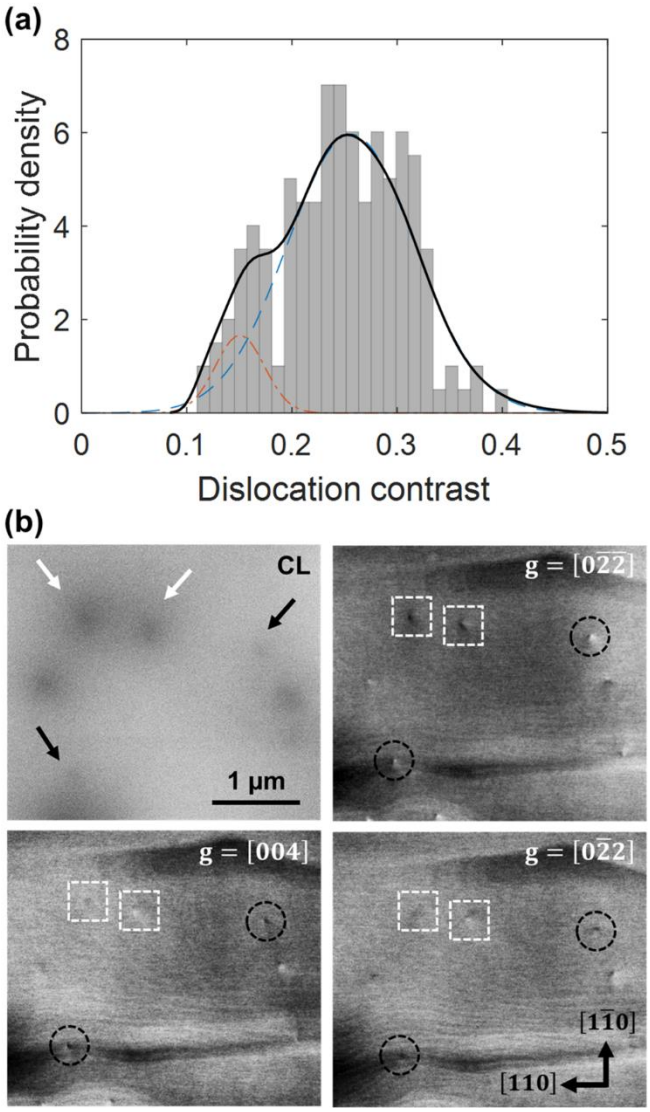

Fig. 8. (a) Histogram and probability density of the CL contrast from ~170 dislocations in the sample grown at 725 °C. (b) Panchromatic CL map from this sample and corresponding two-beam electron channeling contrast images at three different reflections. The white and black arrows represent dislocations with strong and weak CL contrast respectively. These same groups of dislocations are highlighted in the ECCI images with white boxes and black circles respectively. The ECCI contrast changes identically for each set of dislocations, indicating that each set has the same Burgers vector.

the recombination velocity S is seen to vary by one order of magnitude, from $4 \times 10^6 cm/s$ (black) to $4 \times 10^7 cm/s$ (white). Comparing the ECCI images, we see that the strong and weak CL contrast dislocations have different Burgers vectors, although the weak CL contrast dislocations themselves have the same Burgers vector, evidenced by their similar contrast across three different

g-vectors. A cursory examination of other weak CL contrast dislocations indicated that they too had Burgers vectors unlike that of the average or strong CL contrast dislocations. However, without the ability to precisely identify the Burgers vector, it was not possible to conclude if they were merely different or also crystallographically different, i.e. screw vs. mixed type. Threading dislocations in a low-mismatch graded buffer with 60° misfit dislocations can be either screw-type or mixed 60°-type and some reports suggest that a majority of threading dislocations are actually of the screw type,[35,36] potentially due to a lower nucleation or multiplication energy. The small bimodality seen in the CL contrast could reflect this asymmetry in threading dislocation types. If this is the case, it would suggest that mixed dislocations have a significantly lower dislocation contrast. Further work on Burgers vector identification via modeling of electron channeling contrast is underway. To summarize, a small fraction of dislocations was observed to have low CL contrast correlated to a distinct Burgers vector. However, the majority of dislocations could not be grouped into subsets based on their CL contrast, indicating that factors other than their Burgers vectors are at play.

IV. DISCUSSION

The key finding of this study is that the recombination activity of threading dislocations in GaInP quantum wells is reduced by lowering the growth temperature. This reduction is facilitated not by a reduction in the carrier diffusion length, but rather a reduction in the recombination strength itself. However, at a growth temperature of 625 °C, the lowest in this study, the luminescence from regions away from dislocations also became weaker, likely due to an increase in the radiative recombination lifetime. We found that at a growth temperature of 675 °C, the dislocation-free luminescence intensity was unaffected (for the excitation level used in this study). This suggests the possibility of optimizing growth conditions specifically for lattice-mismatched samples, these

will likely vary with factors such as source and chamber cleanliness and the excitation level of the device.

The similarity of the CL contrast as a function of temperature rules out the possibility of an energy barrier around dislocations in the 675 °C and 625 °C samples. Such a barrier might have existed if GaInP were disordered near the vicinity of the dislocation due to disruptions in surface processes that lead to ordering. The band gap of the disordered core would have been several tens of meV higher than that of the ordered matrix, thus acting as a barrier. This would manifest as increased CL contrast with increasing temperature as compared with a sample with no barrier, as more carriers would overcome this barrier. This was not observed.

A more likely mechanism for reduced dislocation recombination activity in samples grown at 675 °C and 625 °C is a change in the concentration or coordination of unknown impurities at the dislocation core, leading to fewer trap states. Several studies have attributed the recombination activity at dislocations in compound semiconductors in some part to an atmosphere of impurities and point defects.[37–42] The maximum electron beam induced current (EBIC) contrast due to recombination at intrinsic states in a dislocation in GaAs has been calculated to be ~0.07, with the greater values measured experimentally attributed to extrinsic states introduced by impurities.[43] Similar results were seen in EBIC analysis of dislocations in silicon[39] and CL analysis of dislocations in GaN.[33] The CL contrast at dislocations measured in this study are high—between 0.1–0.4 for the sample grown at 725 °C, but dropping to 0.05–0.15 at 625 °C. At 725 °C, it is possible that impurities have sufficient energy to interact with the dislocation core and incorporate in some configuration that lead to non-radiative states. Whether these impurities migrated to the dislocation from the vicinity is not clear, as no bright halo is observed in CL around each dislocation which should now be free of these impurities. However, it is possible that these

impurities possess only shallow states in the bulk and are not non-radiative in nature, but only become non-radiative after interaction with the dislocation core. At the intermediate temperature of 675 °C, either the migration of impurities to the dislocation or their reaction with the core could be reduced due to slow kinetics. At 625 °C, these are further reduced, leading to very little recombination at the core, becoming close to that predicted for 'clean' dislocations. The large variability in dislocation contrast despite only two crystallographically distinct types of threading glissile dislocations in zincblende III-V materials, screw and mixed, also supports the role of external factors such as impurities. Preliminary data showing a slight bimodality suggests that the Burgers vector could also have a role to play. After all, point defects and impurities are attracted to the dislocation core due to elastic and electrostatic interactions, both dependent on the structure of the dislocation. While the prospect of inducing carrier localization by increasing the microstructural inhomogeneity was not realized in GaInP, it might yet be useful in other material systems where ordering-related lifetime changes do not occur.

V. CONCLUSIONS

We show that the non-radiative recombination strength of dislocations in epitaxial GaInP quantum wells at room temperature is not a fixed value, instead reducing as the growth temperature is reduced. Point defects or impurities are implicated in the recombination process at dislocations from their inability to decorate the dislocation core at lower growth temperatures. Preliminary results also show a role of the Burgers vector in a minority of cases. These results were obtained using a combination of ECCI and CL, with an initial aim to induce carrier localization away from dislocations by ordering and phase separation in GaInP. While no reduction in the diffusion length was seen, likely due to the balancing of lowered carrier diffusivity and longer carrier lifetimes, a marked anisotropy in diffusion due such microstructural change was clearly observed in the non-

radiative recombination. Together, these results highlight the need for growth recipes that are specifically tuned for lattice-mismatched growths and dislocation-filter designs that can control the type of threading dislocations present in the epilayers. Such efforts will be complementary to ongoing efforts in reducing the threading dislocation density and can form an important tool to enable defect-tolerant devices.

ACKNOWLEDGEMENTS

This study made use of the Substrate Engineering Laboratory and the MRSEC Shared Experimental Facilities at MIT, partly supported by the National Science Foundation under Award No. DMR-08-19762.

REFERENCES

[1] F. Schaffler, D. Tobben, H.-J. Herzog, G. Abstreiter, and B. Hollander, Semicond. Sci. Technol. **7**, 260 (1992).
[2] N. Waldron, G. Wang, N.D. Nguyen, T. Orzali, C. Merckling, G. Brammertz, P. Ong, G. Winderickx, G. Hellings, G. Eneman, M. Caymax, M. Meuris, N. Horiguchi, and A. Thean, ECS Trans. **45**, 115 (2012).
[3] R.M. France, F. Dimroth, T.J. Grassman, and R.R. King, MRS Bull. **41**, 202 (2016).
[4] S. Pimputkar, J.S. Speck, S.P. Denbaars, and S. Nakamura, Nat. Photonics **3**, 180 (2009).
[5] J.S. Speck and S.J. Rosner, Phys. B Condens. Matter **273**–**274**, 24 (1999).
[6] A.Y. Liu, C. Zhang, J. Norman, A. Snyder, D. Lubyshev, J.M. Fastenau, A.W.K. Liu, A.C. Gossard, and J.E. Bowers, Appl. Phys. Lett. **104**, 041104 (2014).
[7] J.D. Lambkin, L. Considine, S. Walsh, G.M. O'Connor, C.J. McDonagh, and T.J. Glynn, Appl. Phys. Lett. **65**, 73 (1994).
[8] P. Morin, M. Pitaval, D. Besnard, and G. Fontaine, Philos. Mag. A **40**, 511 (1979).
[9] B.A. Simkin and M.A. Crimp, Ultramicroscopy **77**, 65 (1999).
[10] Y.N. Picard, J.D. Caldwell, M.E. Twigg, C.R. Eddy, M.A. Mastro, R.L. Henry, R.T. Holm, P.G. Neudeck, A.J. Trunek, and J.A. Powell, Appl. Phys. Lett. **91**, 094106 (2007).
[11] S.D. Carnevale, J.I. Deitz, J.A. Carlin, Y.N. Picard, M. De Graef, S.A. Ringel, and T.J. Grassman, Appl. Phys. Lett. **104**, 232111 (2014).
[12] Y.N. Picard, M. Liu, J. Lammatao, R. Kamaladasa, and M. De Graef, Ultramicroscopy **146**, 71 (2014).
[13] K.K. Sabelfeld, V.M. Kaganer, C. Pfüller, and O. Brandt, J. Phys. Appl. Phys. **50**, 405101 (2017).
[14] R.R. King, J.H. Ermer, D.E. Joslin, M. Haddad, J.W. Eldredge, N.H. Karam, B. Keyes, and R.K. Ahrenkiel, in *Proc. 2nd World Conf. Photovolt. Sol. Energy Convers.* (1998).

[15] S.J. Rosner, E.C. Carr, M.J. Ludowise, G. Girolami, and H.I. Erikson, Appl. Phys. Lett. **70**, 420 (1997).
[16] E.B. Yakimov, J. Alloys Compd. **627**, 344 (2015).
[17] H. Demers, N. Poirier-Demers, A.R. Couture, D. Joly, M. Guilmain, N. de Jonge, and D. Drouin, Scanning **33**, 135 (2011).
[18] T. Suzuki, A. Gomyo, and S. Iijima, J. Cryst. Growth **93**, 396 (1988).
[19] K. Mukherjee, P.B. Deotare, and E.A. Fitzgerald, Appl. Phys. Lett. **106**, 142109 (2015).
[20] J.E. Fouquet, V.M. Robbins, S.J. Rosner, and O. Blum, Appl. Phys. Lett. **57**, 1566 (1990).
[21] R.A.J. Thomeer, F.A.J.M. Driessen, and L.J. Giling, Appl. Phys. Lett. **66**, 1960 (1995).
[22] A. Sasaki, K. Tsuchida, Y. Narukawa, Y. Kawakami, S. Fujita, Y. Hsu, and G.B. Stringfellow, J. Appl. Phys. **89**, 343 (2001).
[23] C.M. Fetzer, R.T. Lee, G.B. Stringfellow, X.Q. Liu, A. Sasaki, and N. Ohno, J. Appl. Phys. **91**, 199 (2002).
[24] R.R. King, C.M. Fetzer, P.C. Colter, K.M. Edmondson, D.C. Law, A.P. Stavrides, H. Yoon, G.S. Kinsey, H.L. Cotal, J.H. Ermer, R.A. Sherif, K. Emery, W. Metzger, R.K. Ahrenkiel, and N.H. Karam, in *Proc. 3rd World Conf. OnPhotovoltaic Energy Convers. 2003* (2003), p. 622–625 Vol.1.
[25] T. Mattila, L.-W. Wang, and A. Zunger, Phys. Rev. B **59**, 15270 (1999).
[26] R.P. Schneider, E.D. Jones, and D.M. Follstaedt, Appl. Phys. Lett. **65**, 587 (1994).
[27] S. Froyen, A. Zunger, and A. Mascarenhas, Appl. Phys. Lett. **68**, 2852 (1996).
[28] K. Mukherjee, D.A. Beaton, T. Christian, E.J. Jones, K. Alberi, A. Mascarenhas, M.T. Bulsara, and E.A. Fitzgerald, J. Appl. Phys. **113**, 183518 (2013).
[29] G. Naresh-Kumar, J. Bruckbauer, P.R. Edwards, S. Kraeusel, B. Hourahine, R.W. Martin, M.J. Kappers, M.A. Moram, S. Lovelock, R.A. Oliver, C.J. Humphreys, and C. Trager-Cowan, Microsc. Microanal. **20**, 55 (2014).
[30] N.M. Haegel, T.J. Mills, M. Talmadge, C. Scandrett, C.L. Frenzen, H. Yoon, C.M. Fetzer, and R.R. King, J. Appl. Phys. **105**, 023711 (2009).
[31] D.J. Friedman, A.E. Kibbler, and J.M. Olson, Appl. Phys. Lett. **59**, 2998 (1991).
[32] C. Donolato, J. Appl. Phys. **84**, 2656 (1998).
[33] M. Albrecht, J.L. Weyher, B. Lucznik, I. Grzegory, and S. Porowski, Appl. Phys. Lett. **92**, 231909 (2008).
[34] J.M. Titchmarsh, G.R. Booker, W. Harding, and D.R. Wight, J. Mater. Sci. **12**, 341 (1977).
[35] C.J. Humphreys, D.M. Maher, D. J. Eaglesham, E.P. Kvam, and I.G. Salisbury, J. Phys. III **1**, 1119 (1991).
[36] P.D. Colbourne and D.T. Cassidy, Appl. Phys. Lett. **61**, 1174 (1992).
[37] T. Sekiguchi and K. Sumino, Jpn. J. Appl. Phys. **26**, L179 (1987).
[38] A. Djemel, J. Castaing, N. Visentin, and M. Bonnet, Semicond. Sci. Technol. **5**, 1221 (1990).
[39] M. Kittler, W. Seifert, and V. Higgs, Phys. Status Solidi A **137**, 327 (1993).
[40] A. Hierro, M. Hansen, L. Zhao, J.S. Speck, U.K. Mishra, S.P. DenBaars, and S.A. Ringel, Phys. Status Solidi B **228**, 937 (2001).
[41] V. Kveder, M. Kittler, and W. Schröter, Phys. Rev. B **63**, 115208 (2001).
[42] E.B. Yakimov, A.Y. Polyakov, I.-H. Lee, and S.J. Pearton, J. Appl. Phys. **123**, 161543 (2017).
[43] J.-L. Farvacque, Mater. Sci. Eng. B **42**, 110 (1996).